EFFECT OF AN OXIDE LAYER ON THE RESULT OF A RING COMPRESSION TEST ON A FUEL CLADDING SAMPLE AFTER A SIMULATED LOCA TRANSIENT

J. DESQUINES, S. GUILBERT
IRSN, PSN-RES/SEREX
Centre de Cadarache, 13115 Saint Paul-Lez-Durance – France

ABSTRACT

The post-quench mechanical resistance of fuel claddings after a Loss of Coolant Accident (LOCA) is affected by oxidation at high temperature. The Ring Compression Test (RCT) with controlled displacement is frequently used by the nuclear industry to evaluate cladding embrittlement.
In this study, single side and two-side oxidized claddings at two different Equivalent Clad Reacted (ECR) levels are analyzed. The experimental data previously obtained in [1] are used in the present paper to explore the failure conditions of RCT. The analysis of the load-displacement records of the RCT tests is conducted thoroughly, and supported by finite element calculations when necessary. The behavior of a RCT is shown to be rather complex with several possible steps in the ring failure process. For very brittle samples, a possible transformation of the ring into two C-shaped specimens is observed in the late stage of the test.
In the early stage of the test, the nucleation of cracks within the oxide layer can modify the sample stiffness. For highly resistant samples, buckling of the oxide layer is observed in compression regions, just before sample plastic deformation. The oxide damage has to be cautiously identified in order to distinguish between a decrease of the sample stiffness and some possible plasticity in the sample.
A key outcome of this study is the mapping of the oxide layer damage versus the applied load or applied stress. A revised procedure to determine the offset strain using ring compression test is then proposed and compared to the usual one.

1. Introduction

During a LOCA thermal-mechanical transient, the fuel claddings can burst during heat-up at a temperature close to 800°C and are subsequently oxidized by the steam environment at higher temperatures. The accident ends with water quenching of the oxidized fuel rods. The two key issues for reactor safety are the core coolability and the potential fuel rod failure during or after the quench. The present study rather addresses cladding embrittlement after high temperature steam oxidation, cool down and water quenching. At this temperature, the environment leads to two sides (**2S**) oxidation at both inner and outer diameter at the vicinity of the burst opening and only single side (**1S**) oxidation at outer diameter far from the burst location. On oxidized surfaces, two successive brittle layers form and are connected to a metallic β-zirconium layer: a zirconia layer and an oxygen enriched α-layer, designated as α(O) in the following. After quenching, the degree of material embrittlement is usually evaluated by mechanical testing of the oxidized samples. Many types of mechanical tests can be performed to check the degree of material embrittlement (see [1]). The Ring Compression Test (**RCT**) is commonly used in the nuclear industry to assess the degree of fuel cladding embrittlement after thermal-mechanical accidental or incidental transient [1-6]. The RCT results generated in [1] are used in the present paper to explore the failure conditions of samples oxidized at 1200°C under steam environment.

2. Main steps of sample damage during a RCT

The result of a mechanical test performed (see [7]) on a pre-oxidized sample and further two-sides oxidized at 900°C, as shown in Fig.1, illustrates the complex behavior of RCT after LOCA transient embrittlement. The load-displacement record in Fig.1 shows a two slopes elastic response of the sample with a slight slope change between 5 and 10 N/mm. When reaching 25 N/mm, the inner sides of the two polar locations form simultaneously through-wall cracks associated with a first load drop of about 70%. The test resumes with two half rings (C-shaped Compression Test samples - **CCT**'s). An equivalent lower stiffness is observed with a new load drop of 50% at about 18 N/mm, associated with the failure of one of the two CCT samples. A final load drop is observed when the last CCT sample breaks apart.

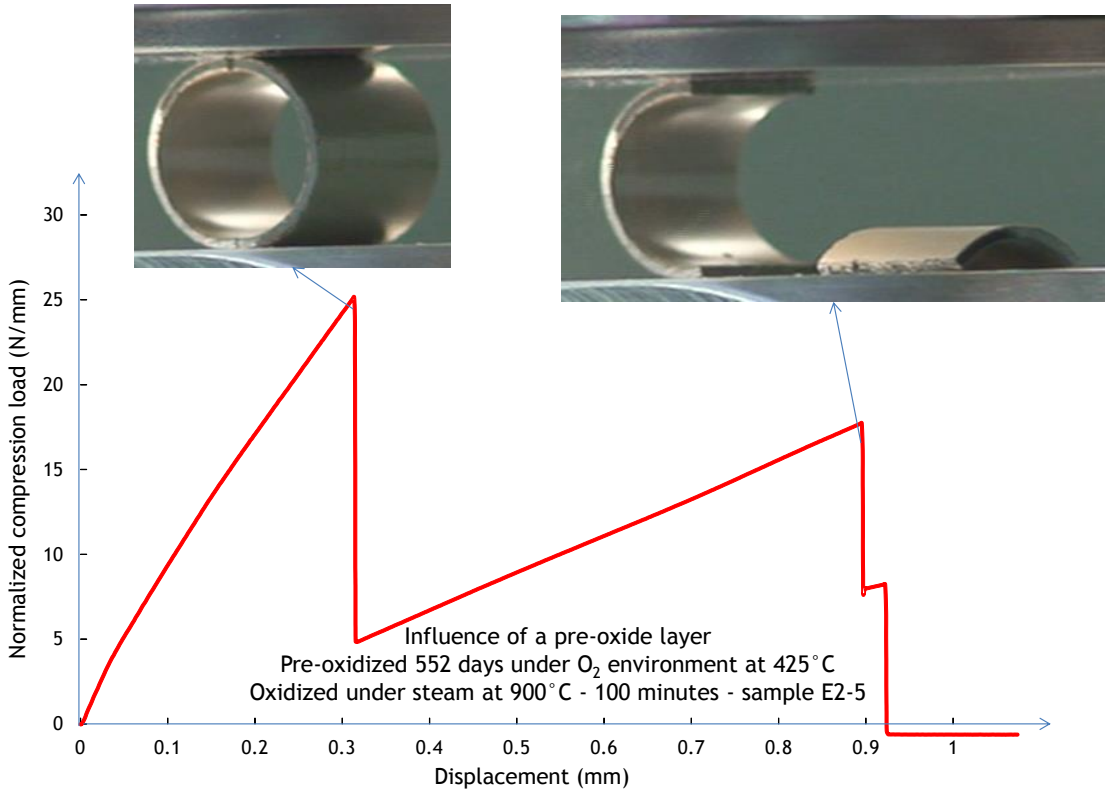

Fig 1. Illustration of load normalized by sample length versus displacement recorded during a RCT performed on a cladding sample after a laboratory simulated LOCA transient (the testing conditions are detailed in [7])

A more general description of the key steps of the sample failure is illustrated in Fig.2. Each step induces a load drop. During the early stage of RCT loading, there are two locations affected by a maximum tensile hoop stress corresponding to Polar (**P**) and Equatorial (**E**) locations. In this early situation, the tangential (hoop) stress at polar location in the inner diameter is approximately 1.75 times higher than the corresponding stress at equatorial location in the outer diameter. But when the sample shape changes after a significant applied displacement without crack nucleation, the maximum stress is located at E and not anymore at P.

As a consequence, for two-sides oxidized RCT samples, two cases can be observed:

- For brittle samples, the cracks are rather nucleated at P on the inner diameter.
- For ductile samples, the cracks are nucleated at E on the outer diameter.
- For intermediate ductility, in some cases, cracks can be nucleated at both E and P locations.

For one side oxidized samples, crack nucleation can only take place at E and outer diameter location with lower dependency to sample embrittlement. Consequently, the evolution of cladding damage strongly depends on both the type of oxidation (1S or 2S) and the degree of material embrittlement.

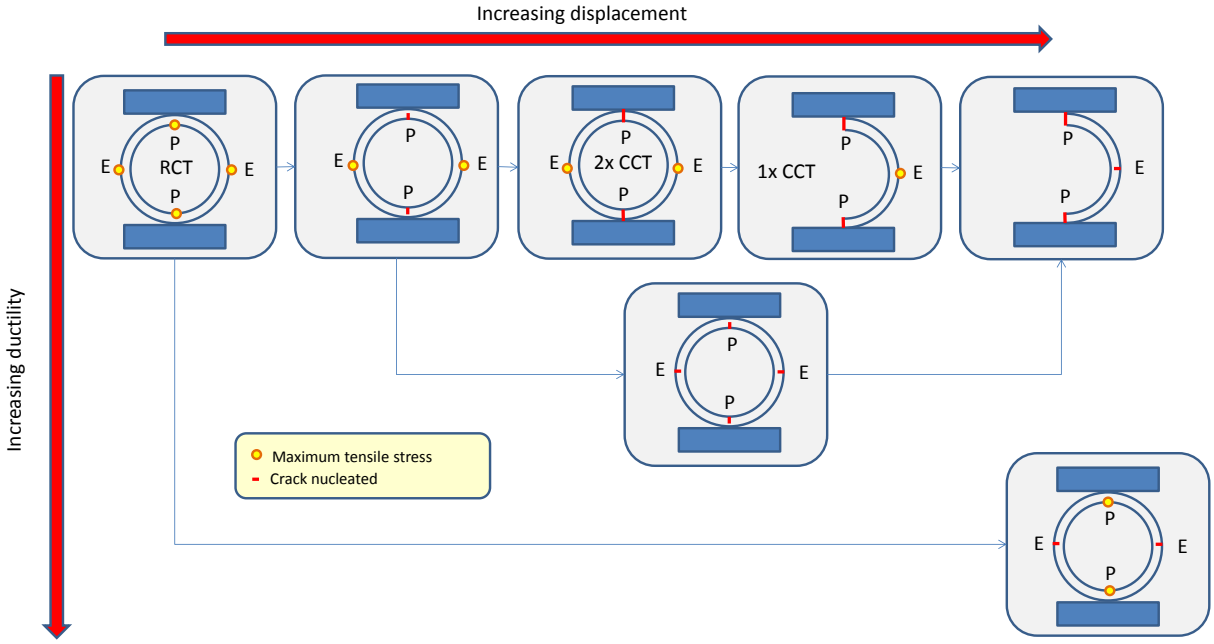

Fig 2. Illustration of the main steps of the RCT damage.

As illustrated in Fig.2, the RCT applied on brittle samples normally ends with CCT testing of the cladding sample. It is consequently extremely interesting to first interpret CCT sample failure conditions and then analyze the RCT test results.

The nucleated crack depth (**a**) corresponds to the cumulated zirconia and α(O) layer thicknesses and the cracks are located in regions affected by tensile stress labelled P or E in Fig.2. The measurement of the various layer thicknesses is fully detailed in [1].

3. Analysis of CCT tests

The load-displacement records of the CCT samples tested in [1] are gathered in Fig.3 with indication of the steam oxidation duration at 1200°C. The results are compared to elastic finite element solutions of a CCT sample with a single radial-axial crack located at the sample outer diameter (E) considering homogeneous Zircaloy-4 cladding and plane strain. The sample stiffness was evaluated using numerically fitted finite element simulations results:

$$\delta^{el} = \frac{F}{L}\frac{1-\nu^2}{E}\left[\frac{1}{2.64.10^{-2}\left(\frac{e}{R_i}\right)^{2.7644}} + 2\frac{a}{e}\left(\frac{R_i}{e}\right)^2\left(0.4 + 58.5\frac{a}{e} + 223.7\left(\frac{a}{e}\right)^4\right)\right] \quad (1)$$

$\delta^{el}(mm)$: elastic displacement at the loading location,
$F/L\ (N/mm)$: applied load divided by sample axial length,
$E(MPa)$= 98829 MPa at room temperature, the Zircaloy-4 Young modulus,
ν=0.345 is the Poisson ratio,
$e\ (mm)$: the oxidized cladding sample thickness (assuming homogeneous material),
$R_i\ (mm)$: inner radius of the oxidized cladding sample,
$a\ (mm)$: depth of the crack located at equatorial location and outer diameter (cumulated zirconia layer thickness and α(O) layer at outer diameter of the sample),
The validity range, with less than 2% error, of the above mentioned equation corresponds to: $\frac{e}{R_i} \in [0.05; 0.25]$ and : $\frac{a}{e} \in [0.0; 0.7]$.

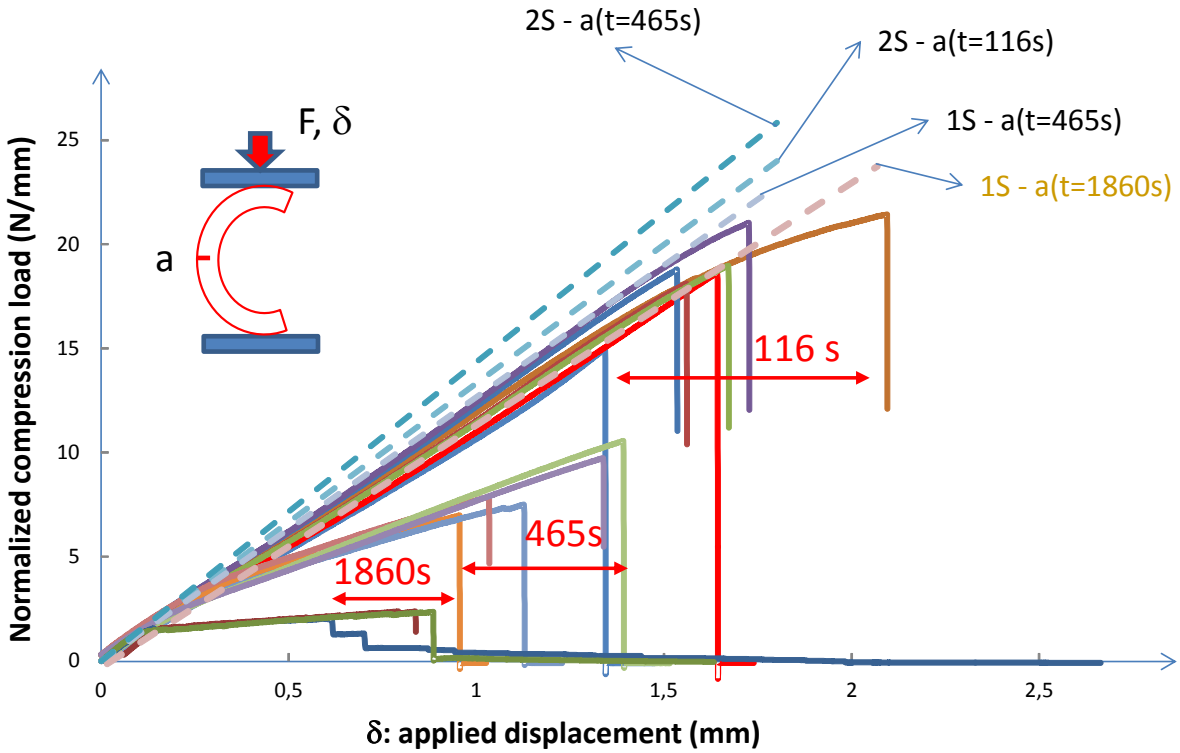

Fig 3. CCT test results (continuous lines) and elastic stiffness (dashed lines) of cracked samples with crack depth (a) depending on steam oxidation duration at 1200°C.

Fig.3 shows a change in the load-displacement slope of the samples. At the beginning of the loading, the sample stiffness is consistent with elastic calculations without cracks. After this, the slope change cannot be explained by the nucleation of a single crack at equatorial location. Elastic calculated stiffness is weakly affected by a single crack nucleation.

In order to clarify the origin of this change of slope, the load-displacement records are compared (see Fig.4) to the calculated sample stiffness when assuming that the outer diameter brittle layer is fully damaged. To obtain this corrected stiffness, the sample thickness is evaluated using equation 1, without contribution of this brittle layer ($e_{corrected} = e - a$) and no crack (a=0).

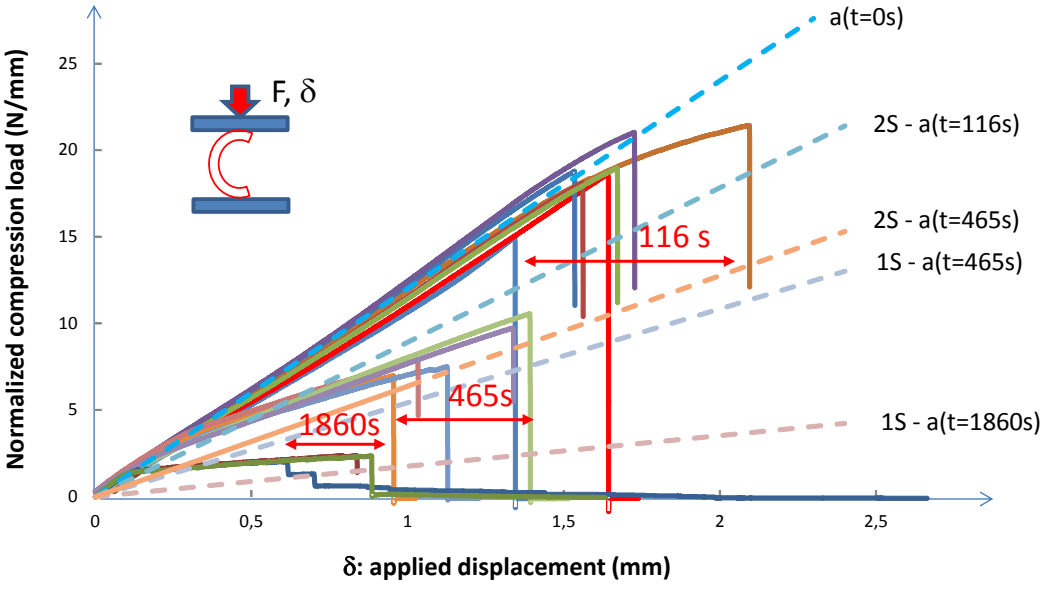

Fig 4. CCT test results (continuous lines) and elastic stiffness (dashed lines) of samples without mechanical contribution of the outer diameter brittle layer.

Fig.4 shows that the calculated modified slopes are rather consistent with the measured slopes after stiffness change. In other words, there is a loading transition level above which the outer diameter brittle layer is fully damaged and does not contribute anymore to the sample stiffness. The observed slope change is not a consequence of the sample plasticity. This result is consistent with the fact that, at a given displacement, the loading level is lower for very brittle samples. Brittle samples are considered harder and, consequently, are expected to have higher yield stress than ductile samples.

4. Analysis of RCT tests

The mechanical behavior of RCT is rather comparable to the one of CCT. Fig.5 plots all the room temperature RCT test results (fully described in [1]) for samples tested after 465 s steam oxidation at 1200°C. At the beginning of the loading, 1S and 2S oxidation samples follow the same trend up to about 10 N/mm. Above this load, the 2S oxidized samples deviate from this trend whereas the 1S oxidized samples follow on with a sample stiffness that is only slightly modified by the load increase. The deviation observed for 2S oxidized samples results from oxide layer and α(O) damage at polar location and inner diameter. These two inner connected brittle layers only exist in the 2S samples. Above 10 N/mm applied load, these layers do not contribute anymore to the sample stiffness resulting in a more compliant sample. Above 50 to 60 N/mm, the 1S sample is first affected by oxide layer spalling in compression regions (small amplitude load drops) and then fails suddenly at both equatorial location keeping contact between the two half's of the sample. The 2S samples fail at each polar location at applied loads between 20 and 30 N/mm. The sample stiffness drastically decreases after this and remains consistent with the stiffness of two CCT's in parallel. The final failure is associated to the failure of each CCT. It is remarkable that the sample stiffness of the corresponding CCT samples is associated to outer brittle layers fully damaged at equatorial location. There are consequently strong connections between CCT and RCT failure processes. Gathering the test results with various testing conditions provides a better understanding of these processes.

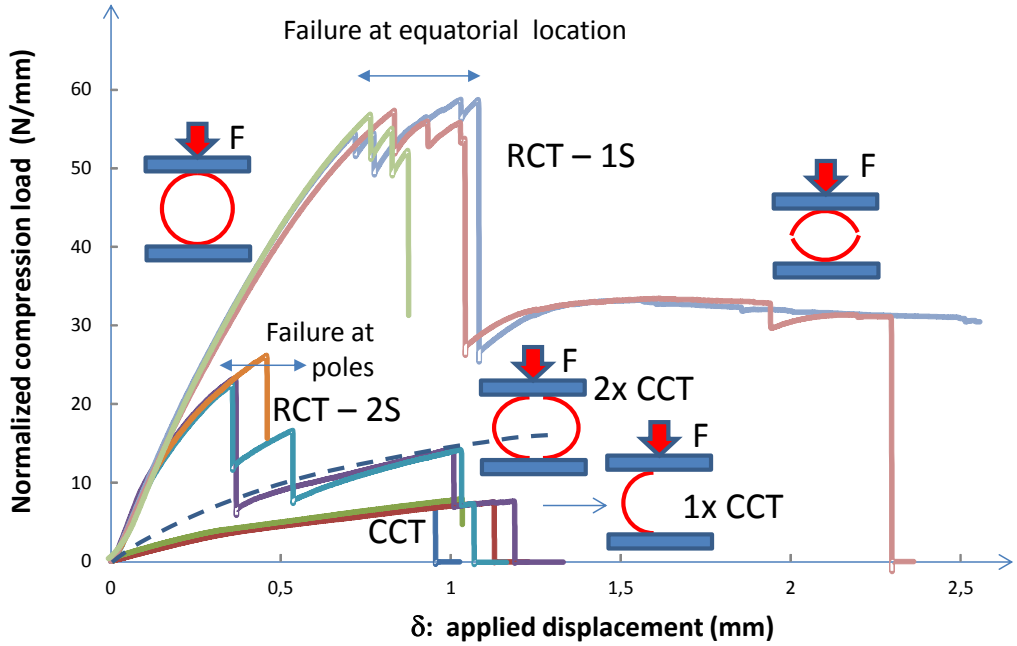

Fig 5. RCT test results (continuous lines) after steam oxidation during 465 s at 1200°C. The dashed line represents two times the load displacement of a CCT oxidized during 465 s. (1S: single side oxidation, 2S: two-side oxidation)

The analysis of other oxidizing conditions is completely similar for samples 2S oxidized during 116 s at 1200°C, as illustrated in Fig.6. One of the 116 s oxidized (green curve in Fig.6) samples confirms oxide spalling at 60 N/mm at load application region. This spalling is associated to the compressive buckling of the oxide layer. The elastic stiffness change is observed above 10 N/mm for both oxidation durations but results in a stronger decrease of sample stiffness for 465 s oxidation than for 116 s oxidation. This result is consistent with thinner embrittled layers after 116 s oxidation than 465 s. The 116 s oxidized samples resisting to loadings above 50 N/mm fail simultaneously at polar location and equatorial location because a lot of elastic energy is released during the sample failure at poles. On the contrary, the 116 s oxidized samples failing at poles for applied loads lower than 50 N/mm are followed by two parallel CCT testing similarly to the observed situation of 465 s oxidized samples.

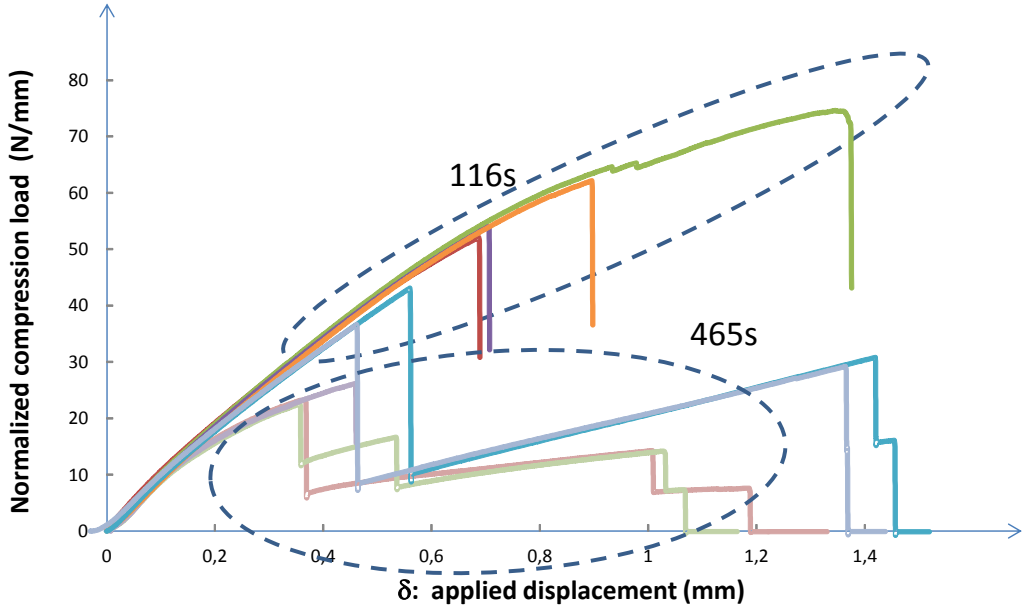

Fig 6. Comparison of the RCT test results after two sides steam oxidation during 116 s and 465 s at 1200°C.

5. Mapping RCT and CCT failure conditions

Only the first load drop conditions (excluding small load drops corresponding to oxide spalling) of a RCT are straightforward analyzed to provide a failure map of the tested samples. Similar conclusions can be drawn for CCT. As illustrated in Fig.7, at very low applied load, and at the polar location, cracks nucleate in the inner diameter oxide layer, changing the sample stiffness. Crack density then increases with the applied load in this brittle layer. When reaching higher load and depending on the oxide layer thickness, the oxide layer located at the loading region (polar location and outer diameter) is affected by a dynamic spalling mode associated to oxide layer buckling under excessive compressive load. Some additional results were extracted from V. Busser PhD thesis [8] confirming this failure mode and its dependency to the outer diameter oxide layer thickness. Above the load required to activate this failure mode, sample plasticity can take place.

This analysis confirms the complexity of RCT load drops that can be affected by different phenomena and must be carefully interpreted. The conditions required to nucleate cracks in the oxide layer are of key importance to determine whether the oxide layer is bearing load or not. Elastic finite element calculations assuming uniform material for the RCT and CCT were used to establish the link between applied load and the stress at inner diameter polar location for RCT and equatorial location and outer diameter for CCT:

$$\sigma_{\theta\theta}^{RCT}(P) = \frac{F}{Le}\left(\frac{6}{\pi}\frac{R_m}{e}\right)\left[1 + 0.3218\left(\frac{e}{R_i}\right) + 0.1362\left(\frac{e}{R_i}\right)^2 - 0.1443\left(\frac{e}{R_i}\right)^3\right] \quad (2)$$

$$\sigma_{\theta\theta}^{CCT}(E) = \frac{F}{Le}\left(6\frac{R_m}{e} - 1\right)\left[1 - 0.4965\left(\frac{e}{R_i}\right) + 0.2548\left(\frac{e}{R_i}\right)^2\right] \quad (3)$$

R_m: is the average radius of the tested sample.
The validity range is: $0 \leq \frac{e}{R_i} \leq 0{,}8$ with less than 1% error on the calculated stress value.

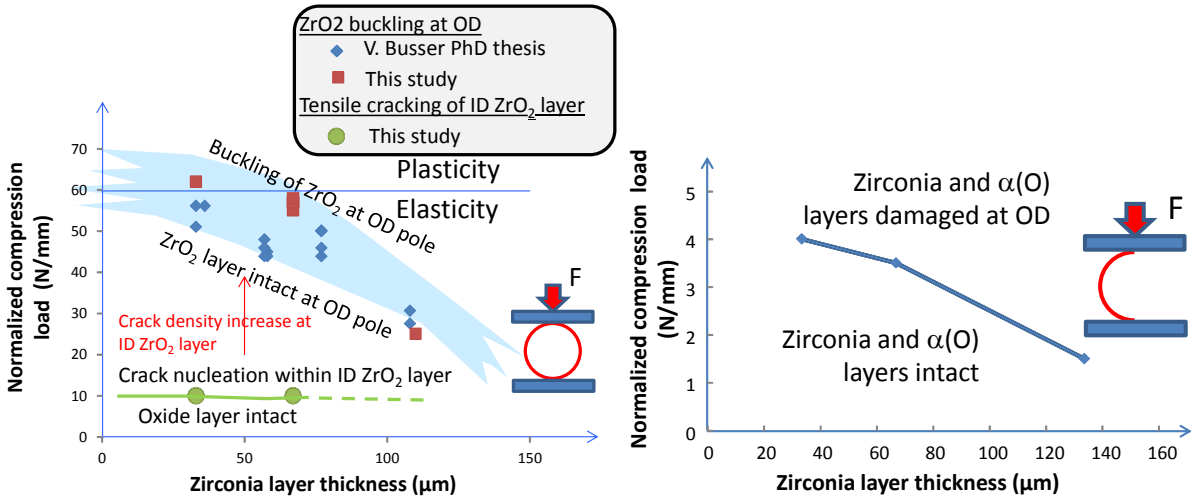

Fig 7. Boundaries of failure modes of a RCT (left) and a CCT (right) (OD is outer diameter, ID is inner diameter).

Fig.8 plots the oxide layer cracking hoop (tangential) stress above which a change in sample stiffness is observed. The results obtained after RCT and CCT tests are plotted together. There is a consistency between the obtained fracture stress values, whatever the type of test used. This result is considered to be a key outcome of the present study.

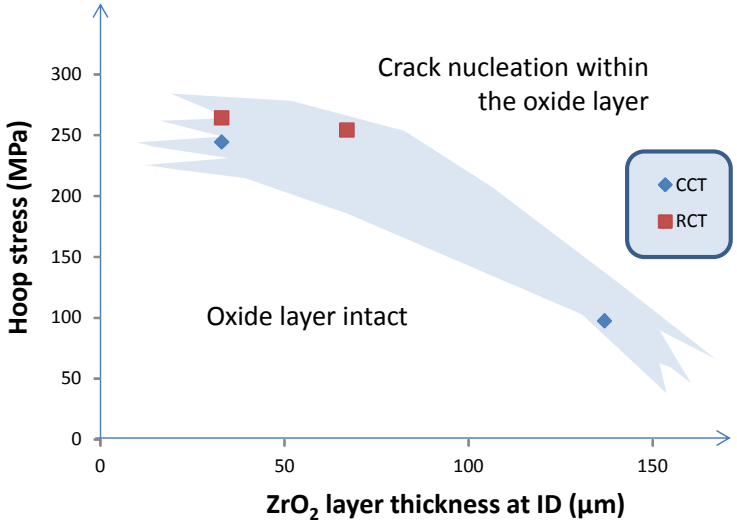

Fig 8. Failure mode of a RCT including oxide layer buckling when oxidized at outer diameter (OD) and oxide layer cracking at inner diameter (ID).

6. Offset strain measurement

The main steps in the load-displacement record are illustrated in Fig.9. Two normalized load thresholds are illustrated, a first one for the oxide layer cracking and a second one for the oxide layer spalling. The offset strain has to be determined using an elastic slope depending

on the measured normalized load at failure (load drop) $\left(\frac{F}{L}\right)_{failure}$ and the measured displacement at failure: $\delta_{failure}$.

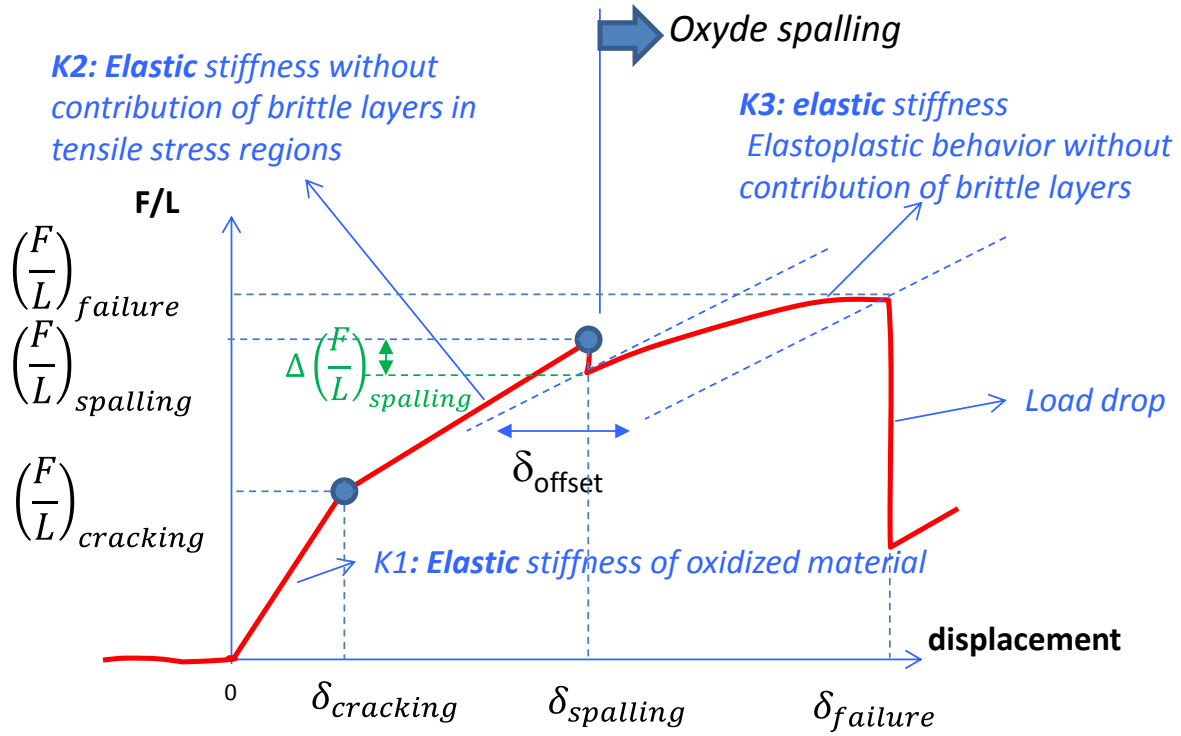

Fig 9. Offset strain assessment using normalized load – displacement record.

The usual procedure is described in detail in [5] and was used in the past at the IRSN. This approach consists in relying on the elastic slope K1 (see Fig.9) to determine the offset displacement using:

$$\delta_{offset} = \delta_{failure} - \frac{1}{K_1}\left(\frac{F}{L}\right)_{failure}$$

The analysis of the RCT and CCT tests described above imply a revised assessment of offset displacement. Three different situations have to be distinguished to determine the offset displacement:

Case 1: $\left(\frac{F}{L}\right)_{failure} \leq \left(\frac{F}{L}\right)_{cracking}$, this situation is theoretically impossible, the sample cannot fail with an intact oxide layer. The offset displacement can be however evaluated using:
$\delta_{offset} = \delta_{failure} - \frac{1}{K_1}\left(\frac{F}{L}\right)_{failure}$.

Case 2: $\left(\frac{F}{L}\right)_{cracking} \leq \left(\frac{F}{L}\right)_{failure} \leq \left(\frac{F}{L}\right)_{spalling}$, then :

$$\delta_{offset} = \delta_{failure} - \delta_{cracking} - \frac{1}{K_2}\left[\left(\frac{F}{L}\right)_{failure} - \left(\frac{F}{L}\right)_{cracking}\right]$$

The offset displacement is expected to be zero without crack propagation in this region.

Case 3: $\left(\frac{F}{L}\right)_{spalling} \leq \left(\frac{F}{L}\right)_{failure}$, then the δ_{offset} measurement is graphically illustrated in Fig.9.

$$\delta_{offset} = \delta_{failure} - \delta_{spalling} - \frac{1}{K_3}\left[\left(\frac{F}{L}\right)_{failure} - \left(\frac{F}{L}\right)_{spalling} + \Delta\left(\frac{F}{L}\right)_{spalling}\right]$$

The oxide spalling can be associated with several minor load drops, and $\Delta\left(\frac{F}{L}\right)_{spalling}$ is the cumulated load drop. The last drop is used to determine the offset displacement. When $\left(\frac{F}{L}\right)_{failure}$ is close to $\left(\frac{F}{L}\right)_{spalling}$, the K_3 slope cannot be accurately evaluated. In this situation the use of K_2 is recommended.

The measured offset strain is straightforward deduced from offset displacement:

$\varepsilon_{offset} = \frac{\delta_{offset}}{D_{sample}}$

D_{sample} is the ring sample diameter.

The obtained offset strains, using either the usual procedure or the revised one, are summarized in Tab.1. The usual procedure leads frequently to non-negligible offset strains at very low applied loads. This unexpected result is corrected using the revised procedure for which offset strain is closer to expected values considering the evolution of plastic strain within the sample. In the usual procedure as developed for RCT, 2% offset strain is recommended as a limit to distinguish brittle from ductile failure. The corresponding limit for CCT tests relying on usual procedure would correspond to approximately 7%. Using the revised procedure, this transition offset strain can be drastically reduced, to about 1%, whatever the type of test.

Procedure		Usual	Revised
Type of test	CCT	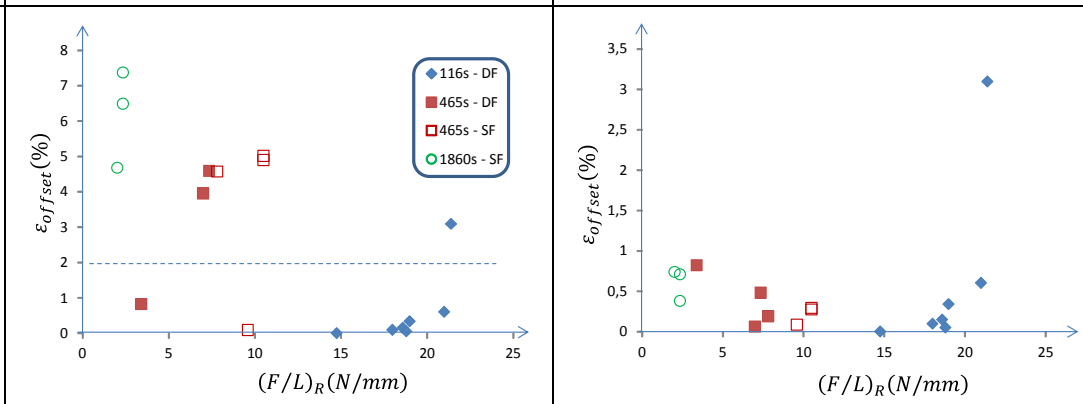	
	RCT	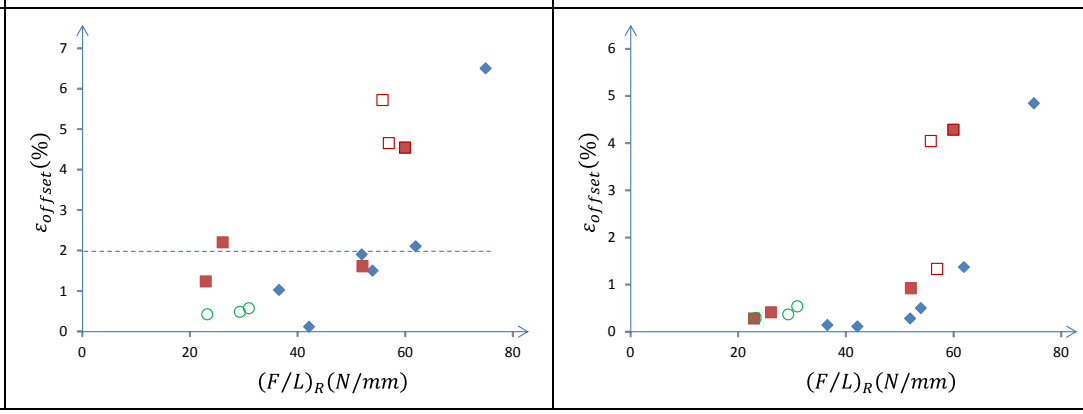	

Tab 1: Comparison between usual and revised procedure to determine offset strains after a simulated LOCA for both CCT and RCT tests.

7. Conclusion

The analysis of the RCT and CCT tests performed in [1] offered the opportunity to a better understanding of the failure mode of ring samples loaded by lateral compression loads. A failure map was provided for RCT and CCT tests showing that the brittle layers induced by high temperature oxidation are cracked over a loading threshold. Above this value, there is another limit associated to oxide layer buckling observed for RCT tests and not for CCT tests.

These damages in brittle layers result in a decreased slope in the load-displacement record during RCT or CCT. The usual procedure dedicated to the determination of offset strains would interpret these slope changes as plasticity. A revised procedure is proposed to distinguish more accurately the specimen plasticity from the damage developing in brittle layers subjected to tensile stress.

5. References

[1] S. Guilbert, J. Desquines, “Fuel Cladding post-quench LOCA Embrittlement: Mechanical test Relevance”, Top Fuel 2016, Boise, ID, September 11-15, 2016.
[2] A. Cabrera, V. Vandenberghe, J. Besson, M. Le Saux, J.-P. Mardon, B. Hafidi, “Finite element modeling of ring compression tests on post-quenched single side oxidized zirconium-based alloys (LOCA conditions)”, Proceedings of 2010 LWR Fuel Performance/Topfuel/WRFPM, Orlando, Florida, USA, September 26-29, 2010.
[3] M.A. Martin-Rengel, F.J. Gomez Sanchez, J. Ruiz-Hervias, L. Caballero, “Determination of the hoop fracture properties of unirradiated hydrogen-charged nuclear fuel cladding from ring compression tests”, Journal of Nuclear Materials, vol. 436, pp.123-129, 2013.
[4] F. Nagase, T. Chuto, T. Fuketa, “Ring compression ductility of high-burnup fuel cladding after exposure to simulated LOCA conditions”, Journal of Nuclear Science and Technology, Vol. 48, No. 11, p. 1369–1376 (2011).
[5] M. Billone, Y. Yan, T. Burtseva, R. Daum, “Cladding embrittlement during postulated Loss-of-Coolant Accidents”, NUREG-CR6967, 2008.
[6] V. Busser, M.-C. Baietto, J. Desquines, C. Duriez, J.-P. Mardon, “Mechanical response of oxidized Zircaloy-4 cladding material submitted to a ring compression test”, Journal of Nuclear Materials, vol. 384, pp. 87-95 (2009).
[7] S. Guilbert, C. Duriez, C. Grandjean, “ Influence of a pre-oxide layer on oxygen diffusion and on post-quench mechanical properties of Zircaloy-4 after steam oxidation at 900°C”, Proceedings of 2010 LWR Fuel Performance/TopFuel/WRFPM, Orlando, Florida, USA, September 26-29, 2010, Paper 121.
[8] V. Busser, “Mécanismes d'endommagement de la couche d'oxyde des gaines de crayons de combustible en situation accidentelle de type RIA », PhD thesis, Defended at INSA de Lyon, 2009.